HHS Public Access

Author manuscript

Lab Chip. Author manuscript; available in PMC 2019 December 04.

Published in final edited form as:

Lab Chip. 2018 December 04; 18(24): 3892–3902. doi:10.1039/c8lc01075g.

On-chip oocyte denudation from cumulus-oocyte complexes for assisted reproductive therapy

Lindong Weng[1,2], **Gloria Y. Lee**[2,3], **Jie Liu**[2,3], **Ravi Kapur**[1,2], **Thomas L. Toth**[4,#], and **Mehmet Toner**[1,2,3,*]

[1]BioMEMS Resource Center, The Center for Engineering in Medicine, Massachusetts General, Hospital and Harvard Medical School, Boston, MA 02129, USA

[2]Department of Surgery, Massachusetts General Hospital and Harvard Medical School, Boston, MA 02114, USA

[3]Shriners Hospital for Children, Boston, MA 02114, USA

[4]Department of Obstetrics and Gynecology, Massachusetts General Hospital and Harvard, Medical School, Boston, MA 02114, USA

Abstract

Human infertility can be treated using assisted reproductive technology (ART) such as intracytoplasmic sperm injection (ICSI). But current ART techniques suffer from multiple cumbersome processes requiring technically skilled personnel. Microfluidics technologies offer unique opportunities to streamline ART procedures, reduce stress imposed upon gametes and embryos, and minimize the operator-to-operator variability. However, there have been no automated and continuous processing systems that can reduce the dependence on well-trained embryologists to obtain ICSI-ready oocytes from patients. In this study, using mouse models, we developed a microfluidic device to denude oocytes from the surrounding cumulus-corona cell mass, facilitating the evaluation of oocyte quality and the injection of sperm. Enzyme-treated cumulus-oocyte complexes pass through a series of jagged-surface constriction microchannels of optimized geometries. The jagged inner wall of constriction channels facilitates to strip off the cumulus-corona cell mass. Oocytes that were denuded by the device showed comparable fertilization and developmental competence compared with mechanical pipetting. The device developed in this study achieves the automation of manual process for oocyte denudation in a continuous flow, as well as improving standardization and ease-of-use. Our denudation-on-a-chip approach requires inexpensive and simple equipment, which represents one step forward towards improving the accessibility and affordability of assisted reproductive therapy.

Graphical Abstract

*To whom correspondence should be addressed. Mehmet Toner, mehmet_toner@hms.harvard.edu.
#Current address: Boston IVF, LLP, Boston, MA 02109, USA

Author Contributions

Conceptualization, L.W., G.Y.L. and M.T.; Methodology, L.W., G.Y.L., J.L. and M.T.; Formal Analysis, L.W., G.Y.L. and J.L.; Investigation, L.W., G.Y.L., J.L. and M.T.; Writing – Original Draft, L.W., G.Y.L., J.L. and M.T.; Writing – Review & Editing, L.W., G.Y.L., J.L., R.K., T.L.T. and M.T.; Supervision, R.K. and T.L.T.; Funding Acquisition, M.T.

Conflict of Interest

The authors declare no conflict of interest.

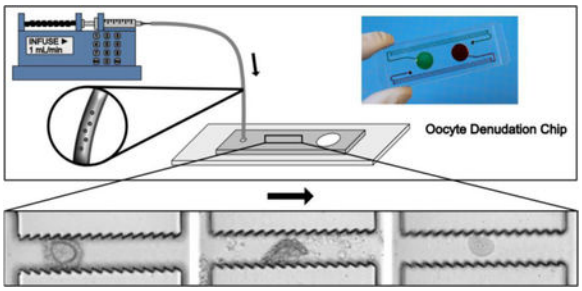

A microfluidic device to denude oocytes from the cumulus-corona cell mass, facilitating the injection of sperm for assisted reproduction therapy

Keywords

Intracytoplasmic sperm injection; *in vitro* fertilization; ART; microfluidics; automation

Introduction

Human infertility has remained a highly prevalent global condition. Infertility is estimated to affect between 8 and 12% of reproductive-aged couples worldwide.[1] In the United States, 1 in 8 couples have trouble getting pregnant or sustaining a pregnancy.[2] The rate of infertility is much higher in the developing regions such as South Asia, Central and Eastern Europe and Central Asia, and Sub-Saharan Africa.[1, 3] For example, the prevalence of infertility is 21.2% in northwestern Ethiopia and between 20 and 30% in Nigeria.[1]

Infertility can be treated using assisted reproductive technology (ART) such as *in vitro* fertilization (IVF) and intracytoplasmic sperm injection (ICSI).[4] According to the Centers for Disease Control and Prevention (CDC), a total of 182,111 ART procedures with the intent to transfer at least one embryo were performed in the United States in 2015, contributing to 1.7% of all infants born in the US during the same year.[5] But current ART procedures like IVF and ICSI still suffer from a variety of limitations,[6] such as being costly and time-consuming.7 The ART procedures also rely heavily on highly skilled embryologists, which often results in variation from operator to operator and the lack of standardization.[6]

To address these challenges, in the past two decades, microfluidic technologies have demonstrated great potential in streamlining the ART procedures.[8]Microfluidics has been successfully integrated with various ART procedures including semen analysis for male infertility diagnosis,[9, 10] sperm selection based on motility[11–15] and/or facilitated by chemotaxis,[16, 17] rheotaxis[18–20] or thermotaxis,[21] oocyte analysis and selection,[22, 23] insemination,[24] embryo culture,[25–27] and cryopreservation.[28–30] Selection of highly motile sperms is crucial for the success of *in vitro* fertilization.[31]As traditional sperm selection methods such as swim-up and centrifugation usually generate low yield of motile sperms or DNA fragmentation,[32]Asghar et al.[13] developed a sperm-sorting device where the most motile and functional sperms can pass through a polycarbonate membrane filter against gravity and swim into a retrieval reservoir on top of the filter, leaving dead and less motile

sperms behind. This device enables the sorting of unprocessed semen sample with higher DNA integrity and fewer reactive oxygen species than traditional sperm selection methods. Recently, a microfluidic device, named the Simple Periodic ARray for Trapping And isolatioN (SPARTAN), utilized an array of pillars to efficiently isolate motile and morphologically normal sperm from raw semen with lower epigenetic global methylation.[15] For ART procedures on female gametes, Han et al.[27] integrated single oocyte trapping, fertilization and embryo culture on a microwell array, enabling automated tracking of the developmental status of each individual embryo. It has also been reported that murine ovarian follicles could produce the human 28-day menstrual cycle hormone profile when mouse ovarian tissue was cultured on a microfluidic platform based on pneumatic actuation, simulating the *in vivo* female reproductive tract and the endocrine loops between organ modules.[33]Other applications of microfluidics in assisted reproductive technology have been reviewed recently.[6–8, 34, 35]

Despite the above breakthroughs in integrating microfluidics with ART procedures, microfluidics technologies have rarely been exploited to improve the processing of oocytes in preparation for ICSI. Intracytoplasmic sperm injection is a dominant treatment to almost all forms of male infertility and has been increasingly adopted to overcome fertilization failure.[36]In 2012, ICSI was used in 93.3% of fresh IVF procedures (embryos transferred without being frozen) with male factor infertility and was used in 76.2% of all fresh IVF procedures with and without male factor infertility.[37]Prior to ICSI, oocytes must be denuded to facilitate the injection of sperm[34] and to allow the evaluation of oocyte morphology, in particular, the nuclear maturation stage.[38] An oocyte is surrounded by cumulus cells, the specialized granulosa cells, forming an organized structure known as the cumulus-oocyte complex (COC). The cumulus cells that are in close contact with the oocyte, also known as corona cells, develop cytoplasmic projections which cross the zona pellucida and form gap junctions with the oolemma.[38] In ART clinics, oocytes must be denuded from the cumulus-corona cell mass, usually via enzymatic action of hyaluronidase and mechanical pipetting, which are inefficient and suffers from the operator-to-operator variation. In a pilot study, Zeringue et al.[39, 40] developed a microfluidic device to mechanically remove the cumulus cell mass from single bovine zygotes. But their device can only process one zygote at a time and requires manual controlling and switching of multiple fluid flows.

In this study, using mouse models, we developed a microfluidic device to denude oocytes from the surrounding cumulus-corona cell mass in a continuous fluid flow. Our device features repeating constriction-expansion units of optimized geometries and surface features to ensure the complete denudation of mouse oocytes while avoiding excessive mechanical stress. Statistically, oocytes that were denuded by our device did not show compromised fertilization or developmental potential compared with the conventional manual denudation protocol. The findings in this study also improve our understanding of the biomechanical mechanisms of oocyte denudation. Furthermore, our oocyte denudation device has the translational potential of processing human samples in an automated, standardized and continuous processing manner in a clinical setting.

Materials and Methods

Device microfabrication

The oocyte denudation chip was fabricated using standard PDMS soft lithography techniques. A single layer master was fabricated by spin-coating SU-8 negative photoresist (Microchem, Newton, MA) onto a silicon wafer. The coated wafer was patterned using UV photolithography to define the master for the chip. The height of SU-8 features was measured to be approximately 275 μm using a surface profilometer (Dektak ST System Profilometer, Veeco Instruments Inc., Plainview, NY). The PDMS prepolymer was mixed with the crosslinker (Dow Corning, Midland, MI) at a ratio of 10:1 (w/w). The mixture was then poured onto the silicon master mold, degassed, and cured at 65°C overnight. The cured PDMS replica was removed from the mold. Inlet and outlet throughholes were punched out for fluidic connection using 2-mm and 10-mm Harris Uni-Core biopsy punchers (Ted Pella, Inc., Redding, CA), respectively. The PDMS slab was treated by oxygen plasma at 300 mmTor oxygen at 50 W for 35 seconds, and then bonded to a 75 mm × 25 mm glass slide to assemble the final oocyte denudation chip.

CFD simulation

To estimate flow profiles and shear stresses within the denudation device and during manual pipetting, CFD models were created using ANSYS Fluent 13 (ANSYS, Inc., Canonsburg, PA). For denudation channels, the model achieved a 0.5, 0.75 or 1 mL/min flow rate using an inlet pressure boundary condition that was 2200, 3492 or 4866 Pa higher than the pressure specified at the outlet boundary, assuming an isotropic constant viscosity of 0.00089 Pa·s for water. To model the denudation device, 5 repeating constriction-expansion units were employed with the full height (275 μm). This resulted in a mesh of over 2.8 million triangular elements. For manual pipetting, the model achieved a 0.5, 0.75 or 1 mL/min flow rate using an outlet pressure boundary condition that was 6222, 9682 or 13386 Pa lower than the pressure specified at the inlet boundary, assuming an isotropic constant viscosity of 0.00089 Pa·s for water. A glass capillary of an outer diameter of 200 μm and an inner diameter of 125 μm was inserted into a 50 μL droplet featuring a semi-spheroid of axes of 4 and 2 mm. The axial length of the glass capillary formed an angle of 30° with the horizontal surface. This resulted in a mesh of more than 1.4 million triangular elements. Each simulation performed 1000 iterations with the residuals dropping below ~10^{-15}.

Acquisition and denudation of germinal-vesicle stage oocytes

All procedures involving animals have been reviewed and approved by the Massachusetts General Hospital Subcommittee on Research Animal Care (no. A3596–01). CF1 female mice (12– 14 weeks old, Charles River Laboratories, Wilmington, MA) were stimulated by intraperitoneal injection of 5 IU of Pregnant Mare Serum Gonadotrophin (PMSG) (ProSpec Protein Specialists, Inc., East Brunswick, NJ). 42–44 hours post PMSG injection, the ovaries were excised from the female mice and place in KSOMaa Evolve w/HEPES medium (LifeGlobal Group LLC, Guilford, CT) at 37 °C. The two ovaries of each mouse were placed in 0.5 mL medium in a center well culture dish (Costar #3260, Corning Inc., Corning, NY). The large follicles of the ovaries were pierced with the tip of a 25-guage needle and pressed to expel the cumulus-oocyte complexes into the dish. All the COCs were collected

into another center well culture dish with fresh 0.5 mL medium. To prepare the COCs for denudation, ~10 COCs were transferred to a 50-μL drop of 0.3 mg/mL hyaluronidase (Sigma-Aldrich, St. Louis, MO) in the same medium, and incubate for 5 minutes. For each denudation experiment, a 10-μL suspension containing about 10 germinal-vesicle (GV) stage COCs were loaded into one end of the Tygon tubing which had been filled with culture media. This end was then connected to a 15-guage blunt needle attached to a 5-mL syringe. The channels and retrieval well on the device had been wetted by flushing 1 mL culture media through the channels before loading COCs. The syringe was mounted on a syringe pump that supplied a constant flow rate of 0.5, 0.75 or 1 mL/min. After about 30 seconds, we collected the processed oocytes from the outlet reservoir using a micropipette with a 1000-μL filter tip (inside diameter of the orifice is about 1.1 mm) and then transferred the volume into a clean petri dish to score the denudation outcome.

Acquisition and denudation of metaphase II stage oocytes

To obtain metaphase II (MII) stage COCs, B6D2F1/J female mice (12–14 weeks old, Jackson Laboratories, Bar Harbor, ME) were injected intraperitoneally with 5 IU PMSG, followed by a second injection of 5 IU Human Chorionic Gonadotropin (HCG) 48 hours later. COC clusters were retrieved from the ampulla of each oviduct 15 to 16 hours after the second injection, and randomly selected to be denuded by a chip or manually. COC clusters were then incubated in 0.3 mg/mL hyaluronidase for 5 minutes before on-chip or manual denudation. For on-chip denudation, each COC cluster was picked up by a stripper pipette and loaded into the inlet tubing connected to a denudation device (W_3=90 μm and N=100) as previously described. A constant flow rate of 1 mL/min was applied. For manual denudation, COC clusters were gently pipetted using a 200 μL pipette tip. The numbers of loaded and retrieved oocytes, as well as the denudation efficiency were recorded. Denuded oocytes were then cultured in KSOMaa medium at 37 °C with 6% CO_2 in humidified air until use.

IVF procedures

To prepare sperm, caudae epididymides were collected from B6D2F1/J male mice. Sperm were released by slicing the epididymides using a 27-gauge needle in fertilization medium.[41] The sperm suspension was collected into a 1.5-mL micro centrifuge tube and incubated at 37 °C with 6% CO_2 for swim up. Ten minutes later, sperm suspension from the top portion of the swim up tube was transferred to a new 1.5-mL tube and the sperm concentration was counted. Seven to nine MII oocytes were washed and transferred to each 50 μL fertilization droplet. Two to four microliters of sperm suspension were added to each 50 μL fertilization drop containing oocytes for a final sperm concentration of 1×10^6 cells/mL. After 4 hours of co-culture, oocytes were removed from fertilization droplets, washed, and cultured in KSOMaa medium. The numbers of two-cell embryos and blastocysts were recorded. Fertilization rate refers to the number of two-cells divided by the number of oocytes inseminated. Blastocyst rate is the percentage of two-cell embryos developed to blastocysts.

ICSI procedures

ICSI was performed as previously described.[42] Briefly, sperm heads and tails were separated by sonication. A single sperm head was picked up by an injection pipette and inserted into an oocyte. Presumptive zygotes were washed and cultured in KSOMaa medium at 37 °C

with 6% CO_2 in humidified air. The numbers of two-cell embryos and blastocysts were recorded. Fertilization rate refers to the number of two-cells divided by the number of oocytes survived injection. Blastocyst rate is the percentage of two-cell embryos developed to blastocysts.

Results and Discussion

Development of oocyte denudation device

In preparation for micromanipulation such as ICSI, oocytes must be denuded from the surrounding cumulus-corona cell mass using a combination of enzymatic and mechanical methods. A handful of hyaluronidase-treated cumulus-oocyte complexes undergo a series of manual pipetting through capillary tips of decreasing inner diameters. As hyaluronidase helps loosen the cumulus extracellular matrix, the shear that COCs experience when being aspirated into the capillary tip is speculated to be responsible for stripping off the cumulus-corona cell mass. Inspired by this hypothetical mechanism, we designed a microfluidic device that features repeating jagged-surface constriction channels, as illustrated in Figure 1 A. This 275-μm thick, single-layer device includes three consecutive sections and each section consists of repeating constriction-expansion units of a given geometry and surface feature. There are 25 constriction-expansion units in each of the first and second sections with widths of the smooth-surface constriction channels (W_1 and W_2) of 240 and 140 μm, respectively (Figure 1 B and C). The third section includes 100 constriction-expansion units, in which the constriction channels have jagged surface and a uniform narrowest width of W_3 (i.e., 90, 100, 110, 120, or 130 μm) (Figure 1 D). It should be noted that the jagged-teeth tilt against the flow direction. In all these three sections, the constriction channels are 640 μm long and the expansion channels are 500 μm long and 500 μm wide. The expansion channels were designed to force the COCs to tumble such that its entire surface can contact the inner walls of the constriction channels in the passage. The first two sections are aimed to remove the bulky, loosely attached cumulus cells and the third section is designed to strip off the corona radiata, the innermost layer of the cells which is directly adjacent to the zona pellucida.

The operation of the denudation device is rather straightforward and has been illustrated in Figure 1 E. A 10-μL suspension containing 7–12 COCs is loaded into a Tygon tubing (inner diameter: 1.27 mm) that has been pre-filled with culture media. The tubing is then connected to a syringe through a 15-gauge blunt needle. The syringe has been mounted on a pump that will apply a constant flow rate of 0.5, 0.75 or 1 mL/min. The other end of the tubing is plugged into the inlet port of the device. After the COCs go through all the constriction-expansion units, they are collected in the outlet reservoir.

Optimization of geometry and flow parameters

We used GV stage oocytes and their associated COCs to optimize the geometric and flow parameters for the denudation device. GV stage COCs feature unexpanded, compact cumulus-corona cell mass (Figure 2 A) while metaphase II (MII) stage ones have expanded, less compact cumulus-corona cell mass with corona cells radiating away from the zona pellucida. Mouse MII stage COCs typically form a large cluster as seen in Figure 2 C. The

optimized parameters obtained with GV stage COCs were used on mature, MII stage COCs for *in vitro* fertilization experiments.

Using GV stage COCs (Figure 2 A), we optimized three major parameters to achieve complete denudation of GV stage oocytes as shown in Figure 2 B. They are: the width (W_3) of jagged-surface constriction channel, the total number (N) of constriction-expansion units in the third section, and the flow rate (Q) that the syringe pump applies. In Figure 2 C-E, we summarize the outcome of denudation achieved by the devices featuring a range of W_3, N and Q. Yield rate is calculated as the percentage of completely or incompletely denuded oocytes retrieved in the outlet reservoir. Denudation efficiency represents the percentage of completely denuded oocytes out of the total number of oocytes retrieved in the outlet. As seen in Figure 2 C-E, almost 100% of the oocytes from COCs that enter the device can be recovered in the outlet reservoir, independent of W_3, N and Q. We suspect that some oocytes or COCs may stick to the hydrophilic inner surface of the tubing. When N=100 and Q=1 mL/min, the mean denudation efficiency decreases from 98.6% to 26.7% as W_3 increases from 90 to 130 μm (Figure 2 C), which indicates that the narrowest constriction must be close to the average size of the cumulus-free oocyte (i.e., ~90 μm in diameter) to perform denudation, which highlights the essential role of the physical contact between COCs and the inner wall.

In addition to W_3, the critical effects of N and Q are also demonstrated in Figure 2 D and E. As seen in Figure 2 D, in the case of W_3=90 μm and Q=1 mL/min, the denudation efficiency decreases dramatically to 28.3% when the number of constriction-expansion units in the third section (N) is reduced to 50. This implies that the complete denudation of oocytes requires adequate constriction-expansion units such that the entire surface of a given COC has the chance to contact the inner wall of the constriction channel.

Although the contact of COCs with the jagged-surface inner wall has been proven to be necessary, it alone does not guarantee a complete denudation. When the flow rate is reduced to 0.5 mL/min, as seen in Figure 2 E, the denudation efficiency is only 22.2%. Even a flow rate of 0.75 mL/min generates a lower denudation efficiency (86.2%) than at 1 mL/min (98.6%). Therefore, in addition to sufficient physical contact, the shear stress that is directly correlated with the flow rate has to be large enough to strip off the cumulus-corona cell mass.

The majority of GV stage COCs have a diameter between 125–150 μm (Figure S1 A in the Supporting Information). We also conducted the denudation experiment on two groups of COCs using the optimal design (i.e., W_3=90 μm, N=100 and θ=141°). One group of small COCs have an average diameter of 125 μm and the other group of large COCs have an average diameter of 175 μm. We found that the effect of COC size on the denudation efficiency was insignificant as seen in Figure S1 B.

To further explore the effect of shear stress, we conducted computational fluid dynamics (CFD) simulations of the fluid flow within the device or through the capillary tip during the manual pipetting. As seen in Figure 2 F, the maximum shear stress is directly correlated with the flow rate. For fluid flow through repeating constriction-expansion units, on one hand,

τ_{max} increases from 64.1 to 163.5 Pa as the flow rate increases from 0.5 to 1 mL/min. The maximum shear occurs at the first pair of teeth after entering the jagged-surface constriction channel as shown in Figure 2 G. On the other hand, τ_{max} increases from 149.8 to 392.0 Pa as the flow rate generated by manual pipetting increases from 0.5 to 1 mL/min. For manual pipetting, the maximum shear occurs at the inner ring of the capillary tip as seen in Figure 2 H. The glass capillary we use in our lab for denudation has an outer diameter of 200 μm and an inner diameter of 125 μm. The typical flow rate applied by our embryologists ranges from 500 to 750 μL/min as estimated from a video recording at 60 frames/second. Given the information shown in Figure 2 F, manual pipetting may apply different shear stress in each up-and-down cycle due to the variation in flow rate, generating a difference in the maximum shear stress of up to 250 Pa between 0.5 and 1 mL/min. But our denudation device is able to keep the shear stress constant due to the constant flow rate applied. The maximum difference in shear stress between on-chip and manual denudation can be as much as 230 Pa in the case of a flow rate of 1 mL/min.

To validate our CFD simulation results, we predicted the shear stress acting on the inner wall of the glass capillary in the fully developed flow region. The shear stress acting on the inner wall at the location that is 2,500 μm from the capillary tip axially is 44.9, 65.5 and 82.5 Pa under a flow rate of 0.5, 0.75 and 1 mL/min, respectively. The shear stress (τ) at this location can also be calculated theoretically based on the Poiseuille's law.[43]

$$\tau = \frac{4\mu Q}{\pi r^3} \quad (1)$$

where μ is the dynamic viscosity of the fluid (i.e., water), Q the flow rate, and r the inner radius of the capillary.

The theoretical calculation obtains the shear stress of 38.7, 58.0 and 77.4 Pa at a flow rate of 0.5, 0.75 and 1 mL/min, respectively, in good agreement with the CFD simulation results, which demonstrates the accuracy of our simulation models.

At MII stage, multiple mouse COCs form a single, tight cluster in the oviduct as shown in Figure 2 I. The cluster of multiple COCs becomes loosen after 5 min incubation with 0.3 mg/mL hyaluronidase at 37 °C. To evaluate the performance of our device under a condition close to the ART clinics, we conducted denudation experiments on MII stage mouse COCs as presented in Figure 2 K. These denuded oocytes were then used in IVF and ICSI experiments to characterize their fertilization and developmental potential. It is clear that our denudation device featuring W_3 =90 μm and N=100 has been sufficient to achieve complete denudation when the hyaluronidase-treated cluster of MII stage COCs goes through it at a flow rate of 1 mL/min. The mean yield rate is 98.9% and the denudation efficiency is 93.7% on average (Figure 2 K).

Role of surface feature of the constriction channel and expansion channel

During the preliminary design stage of our denudation device, we found that none of the corona cells could be removed from the oocytes if the interior surface of the constriction

channel is smooth. To investigate how the surface feature of the constriction channel can affect the denudation performance, we introduced θ, the angle between the flow direction and the median line of the tooth (Figure 3 A). As θ increases from 0° to 141°, the teeth of the jagged-surface inner wall change from tilting along the flow direction to tilting against the flow direction. Figure 3 B and C show the yield rate and denudation efficiency of the device featuring different θ. It is evident that the yield rate is independent of θ. But it seems that only the jagged inner wall featuring θ>90°, in this case, θ=141°, is able to 'shave' off the corona cells completely. It should be noted that the flow rate is 1 mL/min and there are 100 repeating constriction-expansion units in the third section with W_3=90 μm. It is suggested that the effect of θ may not be related to the shear stress. Our CFD simulations estimate that the maximum shear stress is 145.3 and 163.5 Pa for θ=39° and 141°, respectively. In both cases, the maximum shear acts at the first tooth when entering the constriction channel. There is also minimal difference in shear between θ=39° and 141° for the rest of the teeth along the channel. The shear stress is 84.1 Pa for the second to last teeth when θ=39° and is 94.7 Pa when θ=141°. Therefore, the shear stress seems not responsible for the significant improvement in denudation efficiency when θ=141° (Figure 3 C).

To further dissect the role of expansion channels in oocyte denudation, we designed another device in which the 100 constriction channels in the third section (each constriction channel is 640 μm long and the narrowest width is 90 μm) are connected end to end without any expansion channels in between, as illustrated in Figure 4 A. This new device has the same first and second sections as those discussed previously. As seen in Figure 4 B, although the yield rate is still close to 100%, the denudation efficiency in the absence of repeating expansion channels becomes less than 20%, highlighting the necessity of expansion channels which may promote the tumbling of COCs. Furthermore, the COCs processed by the device that is illustrated in Figure 4 A typically have an appearance of exposed zona pellucida on one or two sides and cumulus-corona cells remaining intact on the other sides in a two-dimensional image (Figure 4 C), suggesting that only certain parts of the COC surface get physical interaction with the inner wall rather than the entire surface. The elimination of expansion channels is related to a decrease in the denudation efficiency.

It should be noted that the oocytes must be completely denuded to facilitate the injection of sperm. Even a small residue of cumulus cells can potentially prevent puncturing of the oocyte membrane from the appropriate position. Therefore, the rate of complete denudation is more relevant to ICSI procedures. Nevertheless, we also provided a breakdown of the denudation outcome in Figure S2 in the Supporting Information.

Mechanisms of oocyte denudation

We recorded the moments of COCs traveling through the jagged-surface constriction channels using a high-speed camera (Phantom 4.2, Vision Research Inc., Wayne, NJ) at 5,000 frames/second, as shown in Figure 5. Within the first several constriction channels in the third section (e.g., the 3rd one), the COCs are able to fill up the whole width of the channel since the channel width W_3(=90 μm) is smaller than the diameter of the COCs. Thus, the cumulus-corona cells are 'shaved' off by the teeth that tilt against the flow direction. As the COCs travel through the intermediate jagged-surface constriction channels

(e.g., the 25th one), only a portion of the cumulus-corona cell mass has been removed. But within the last several jagged-surfaceconstriction channels (e.g., the 97th one), the cumulus-corona cells are able to be removed completely and a clean oocyte can be seen. Overall, it is evident that the width and number of jagged-surface constrictions (W_3 and N), the flow rate (Q), the teeth titling angle (θ) and the presence of expansion breaks need work synergistically to achieve the complete denudation of oocytes from the surrounding cumulus-corona cell mass.

In the present study, the device only processed COCs. The hyaluronidase-treated cumulus cell layers tend to disperse into single cells or small clusters of cells under appropriate shear stress. These small clusters of cumulus cells, as seen in the middle panel of Figure 5, are too small to cause clogging in the fast-flowing current inside the channels. However, optimization of the design would be necessary for the device to process clinical samples where debris includes blood clots and tissue remnants that may remain intact in response to enzymatic treatment and mechanical stress.

Fertilization and developmental potential of oocytes denuded on a chip

It is of ultimate importance to ensure that the on-chip denudation process does not damage the fertilization and development potential of the denuded oocytes. Therefore, we compared IVF and ICSI procedures using the oocytes denuded by our device and those denuded by manual pipetting. The rate of fertilization, indicated by two-cell formation, and the blastocyst development rate have been shown in Figure 6. The fertilization rate is the percentage of survived oocytes developed to two-cell embryos and the blastocyst rate is the percentage of two-cell embryos developed to blastocysts. Overall, it is evident that the fertilization and development potential of oocytes is not damaged after the cumulus-corona cell mass is removed by our device, as compared with theresults of manual pipetting. For example, the mean fertilization rate and blastocyst rate for IVF is 68.7% and 96.3% when the oocytes are denuded on a chip, compared with 63.1% and 93.1%, respectively, when the oocytes are denuded manually, which are not statistically significant (P=0.52>0.05 and P=0.33>0.05, unpaired $t$test). Similarly, the mean fertilization rate and blastocyst rate for ICSI is 95.9% and 75.5% when the oocytes are denuded on a chip, compared with 88.4% and 76.7%, respectively, when the oocytes are denuded manually, which are also statistically insignificant (P=0.14>0.05 and P=0.84>0.05, unpaired t test). For each repeat of either IVF or ICSI experiment, the on-chip and manual denudation procedures were conducted on parallel on the same day. IVF or ICSI was then performed using the sperm from the same male mouse. The details of our IVF and ICSI experiments have been summarized in Table S1 and S2 in the Supporting Information. Figure 6 E–H display the representative images of two-cell embryos and blastocysts fertilized by either IVF or ICSI.

Conclusions

As the major treatment of infertility, ARTs have not offered sufficient accessibility or affordability to most infertile couples worldwide. Automation and streamlining of ART procedures, such asICSI, are promising approaches in reducing cost and improving the availability of assisted reproductive therapy, especially in resource-limited regions. In this

study, we developed a microfluidic device to process murine cumulus-oocyte complexes in a continuous flow in preparation for ICSI, featuring repeating jagged-surface constriction-expansion units. After theoptimization of the geometry, fluid flow and surface feature, we identified several essential factors for a successful oocyte denudation device. The constriction channel should have a width that is close to the diameter of the cumulus-free oocytes, which ensures the intimate contact between the cumulus-corona cell mass and the inner wall of the constriction channel, and the number of repeating constriction-expansion units needs to be large enough to allow the entire COC surface to have the chance to physically interact with the inner wall of the constriction channel. The COC suspension needs to flow through the device at a rate that can generate sufficient shear to strip off the cumulus-corona cells. We have also shown that the teeth of the jagged-surface inner wall of the constriction channel need to be tilted against the flow direction to enable them to ‘shave’ off the cumulus-corona cells. Finally, the presence of expansion breaks is essential to promote the tumbling of COCs, thus increasing the chance of the entire COC surface to interact with the inner wall. All these factors work synergistically for the complete denudation of oocytes. The device has also been successfully operated by biologists after minimal training who are not specialized in working with microfluidics. Our oocyte denudation device, which has the potential of scaling up, can improve automation and increase efficiency of current ART procedures.

Supplementary Material

Refer to Web version on PubMed Central for supplementary material.

Acknowledgements

We are grateful to Octavio Hurtado for microfabrication assistance and to Dr. Jon Edd for guidance in CFD simulation and high-speed imaging. This work was financially supported by NIH P41 EB002503 and Shriners Hospital for Children (No. 8540). L.W., G.Y.L. and M.T. have submitted a patent application (US62/652,648) for the work described.

References

1. Ombelet W, Cooke I, Dyer S, Serour G and Devroey P, Hum. Reprod. Update, 2008, 14, 605–501621. [PubMed: 18820005]
2. Lepkowski JM, Mosher WD, Davis KE, Groves RM and Van JH, Vital Health Stat 2, 2010, 503 150, 1–36.
3. Mascarenhas MN, Flaxman SR, Boerma T, Vanderpoel S and Stevens GA, PLoS Med, 2012, 505 9, e1001356.
4. Katz P, Nachtigall R and Showstack J, Nat. Med, 2002, 8, 29–32.
5. Sunderam S, Kissin DM, Crawford SB, Folger SG, Boulet SL, Warner L and Barfield WD, MMWR Surveill. Summ, 2018, 67, 1.
6. Kashaninejad N, Shiddiky MJA and Nguyen NT, Adv. Biosyst, 2018, 2, 1700197.
7. Nosrati R, Graham PJ, Zhang B, Riordon J, Lagunov A, Hannam TG, Escobedo C, Jarvi K and Sinton D, Nat. Rev. Urol, 2017, 14, 707. [PubMed: 29089604]
8. Swain J, Lai D, Takayama S and Smith G, Lab Chip, 2013, 13, 1213–1224. [PubMed: 23400523]
9. Schaff UY, Fredriksen LL, Epperson JG, Quebral TR, Naab S, Sarno MJ, Eisenberg ML and Sommer GJ, Fertil. Steril, 2017, 107, 358–364. e354. [PubMed: 27887718]
10. Kanakasabapathy MK, Sadasivam M, Singh A, Preston C, Thirumalaraju P, Venkataraman M, Bormann CL, Draz MS, Petrozza JC and Shafiee H, Sci. Transl. Med, 2017, 9, eaai7863.

11. Zhang X, Khimji I, Gurkan UA, Safaee H, Catalano PN, Keles HO, Kayaalp E and Demirci U, Lab Chip, 2011, 11, 2535–2540. [PubMed: 21677993]
12. Tasoglu S, Safaee H, Zhang X, Kingsley JL, Catalano PN, Gurkan UA, Nureddin A, Kayaalp E, Anchan RM and Maas RL, Small, 2013, 9, 3374–3384. [PubMed: 23677651]
13. Asghar W, Velasco V, Kingsley JL, Shoukat MS, Shafiee H, Anchan RM, Mutter GL, Tüzel E and Demirci U, Adv. Healthc. Mater, 2014, 3, 1671–1679. [PubMed: 24753434]
14. Nosrati R, Vollmer M, Eamer L, San Gabriel MC, Zeidan K, Zini A and Sinton D, Lab Chip, 2014, 14, 1142–1150. [PubMed: 24464038]
15. Chinnasamy T, Kingsley JL, Inci F, Turek PJ, Rosen MP, Behr B, Tüzel E and Demirci U, Adv. Sci, 2018, 5, 1700531.
16. Kricka L, Nozaki O, Heyner S, Garside W and Wilding P, Clin. Chem, 1993, 39, 1944–1947. [PubMed: 8375079]
17. Xie L, Ma R, Han C, Su K, Zhang Q, Qiu T, Wang L, Huang G, Qiao J and Wang J, Clin. Chem, 2010, 56, 1270–1278. [PubMed: 20551382]
18. Cho BS, Schuster TG, Zhu X, Chang D, Smith GD and Takayama S, Anal. Chem, 2003, 75, 1671–1675. [PubMed: 12705601]
19. Seo D.-b., Agca Y, Feng Z and Critser JK, Microfluid. Nanofluidics, 2007, 3, 561–570.
20. Chen Y-A, Huang Z-W, Tsai F-S, Chen C-Y, Lin C-M and Wo AM, Microfluid. Nanofluidics, 2011, 10, 59–67.
21. Li Z, Liu W, Qiu T, Xie L, Chen W, Liu R, Lu Y, Mitchelson K, Wang J and Qiao J, Biomicrofluidics, 2014, 8, 024102. [PubMed: 24803958]
22. Zeggari R, Wacogne B, Pieralli C, Roux C and Gharbi T, Sens. Actuators B Chem, 2007, 125, 664–671.
23. Angione SL, Oulhen N, Brayboy LM, Tripathi A and Wessel GM, Fertil. Steril, 2015, 103, 281–290. e285. [PubMed: 25450296]
24. Suh RS, Zhu X, Phadke N, Ohl DA, Takayama S and Smith GD, Hum. Reprod, 2006, 21, 477–483. [PubMed: 16199424]
25. Ma R, Xie L, Han C, Su K, Qiu T, Wang L, Huang G, Xing W, Qiao J and Wang J, Anal. Chem, 2011, 83, 2964–2970. [PubMed: 21438638]
26. Heo YS, Cabrera LM, Bormann CL, Smith GD and Takayama S, Lab Chip, 2012, 12, 2240–2246. [PubMed: 22402469]
27. Han C, Zhang Q, Ma R, Xie L, Qiu T, Wang L, Mitchelson K, Wang J, Huang G and Qiao J, Lab Chip, 2010, 10, 2848–2854. [PubMed: 20844784]
28. Lai D, Ding J, Smith G, Smith G and Takayama S, Hum. Reprod, 2014, 30, 37–45. [PubMed: 25355589]
29. Song YS, Moon S, Hulli L, Hasan SK, Kayaalp E and Demirci U, Lab Chip, 2009, 9, 1874–1881. [PubMed: 19532962]
30. Heo YS, Lee H-J, Hassell BA, Irimia D, Toth TL, Elmoazzen H and Toner M, Lab Chip, 2011, 11, 3530–3537. [PubMed: 21887438]
31. Knowlton SM, Sadasivam M and Tasoglu S, Trends Biotechnol, 2015, 33, 221–229. [PubMed: 25798781]
32. Henkel RR and Schill W-B, Reprod. Biol. Endocrinol, 2003, 1, 108. [PubMed: 14617368]
33. Xiao S, Coppeta JR, Rogers HB, Isenberg BC, Zhu J, Olalekan SA, McKinnon KE, Dokic D, Rashedi AS and Haisenleder DJ, Nat. Commun, 2017, 8, 14584. [PubMed: 28350383]
34. Smith GD and Takayama S, Mol. Hum. Reprod, 2017, 23, 257–268. [PubMed: 28130394]
35. Yanez LZ and Camarillo DB, Mol. Hum. Reprod, 2017, 23, 235–247. [PubMed: 27932552]
36. Palermo G, Joris H, Devroey P and Van Steirteghem AC, Lancet, 1992, 340, 17–18. [PubMed: 1351601]
37. Boulet SL, Mehta A, Kissin DM, Warner L, Kawwass JF and Jamieson DJ, JAMA, 2015, 313, 255–263. [PubMed: 25602996]
38. Rienzi L, Balaban B, Ebner T and Mandelbaum J, Hum. Reprod, 2012, 27, i2–i21. [PubMed: 22811312]

39. Zeringue H, Beebe D and Wheeler M, Biomed. Microdevices, 2001, 3, 219–224.
40. Zeringue H, Rutledge J and Beebe D, Lab Chip, 2005, 5, 86–90. [PubMed: 15616744]
41. Li M-W, Glass OC, Zarrabi J, Baker LN and Lloyd KK, J. Fertili. In Vitro, 2016, 4.
42. Liu J, Lee G, Lawitts J, Toner M and Biggers J, J. Anim. Sci, 2012, 90, 3739–3742. [PubMed: 22665678]
43. Malek AM, Alper SL and Izumo S, JAMA, 1999, 282, 2035–2042. [PubMed: 10591386]

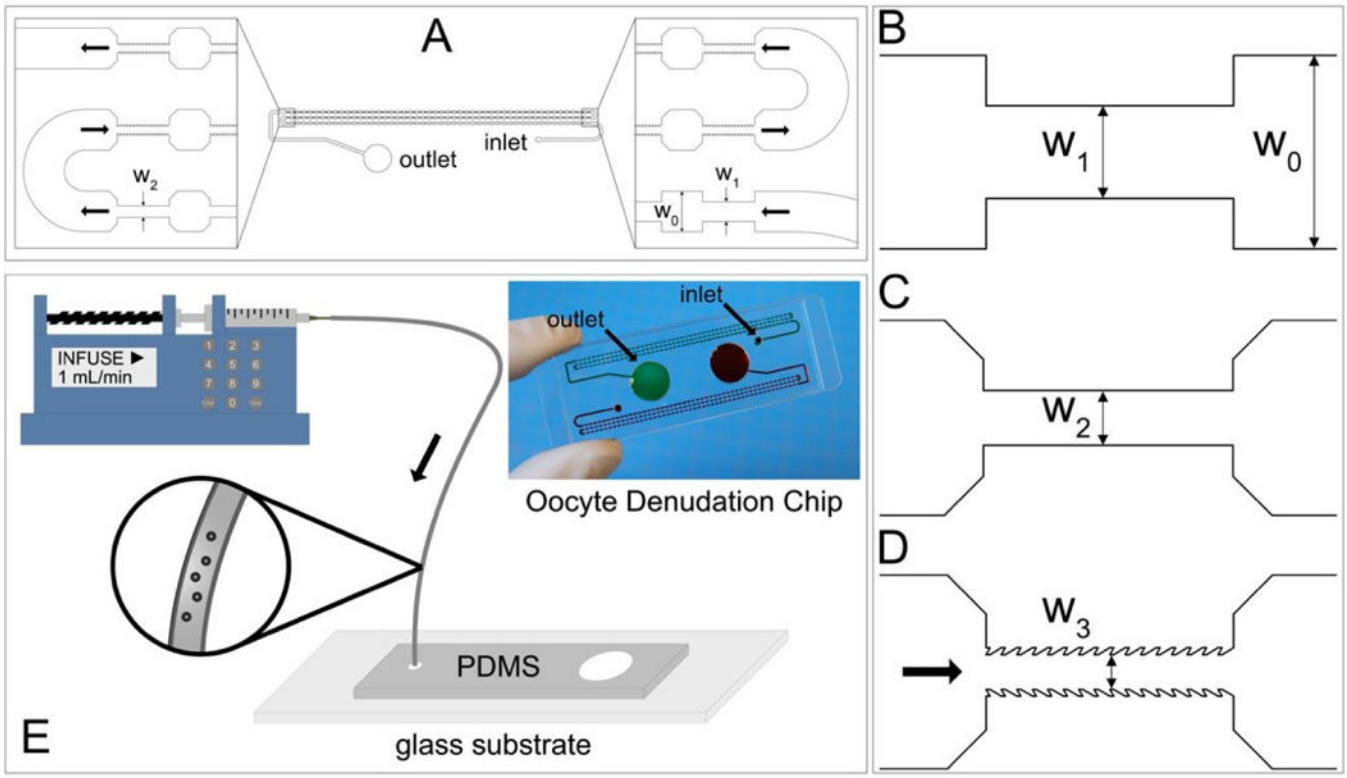

Figure 1.

Design and operation of the oocyte denudation device. (A-D) Schematic diagrams of the repeating constriction-expansion channels. The height of all the channels is 275 μm and the width (W_0) of all the expansion channels is 500 μm. The first 25 constrictions have a width (W_1) of 240 μm (B) and the second 25 constrictions have a width (W_2) of 140 μm (C). All the first 50 constrictions feature smooth surface. The following 100 constrictions feature jagged surface and a width of W_3 that is 90, 100, 110, 120, or 130 μm (D). (E) The operation of the oocyte denudation device involves a syringe pump applying a constant flow and a Tygon tubing (ID: 1.27 mm) pre-loaded with COCs suspended in the medium. Inset: A photograph of a PDMS-glass chip in which two sets of the denudation devices shown in (A) are bonded to a single 75 mm x 25 mm glass slide.

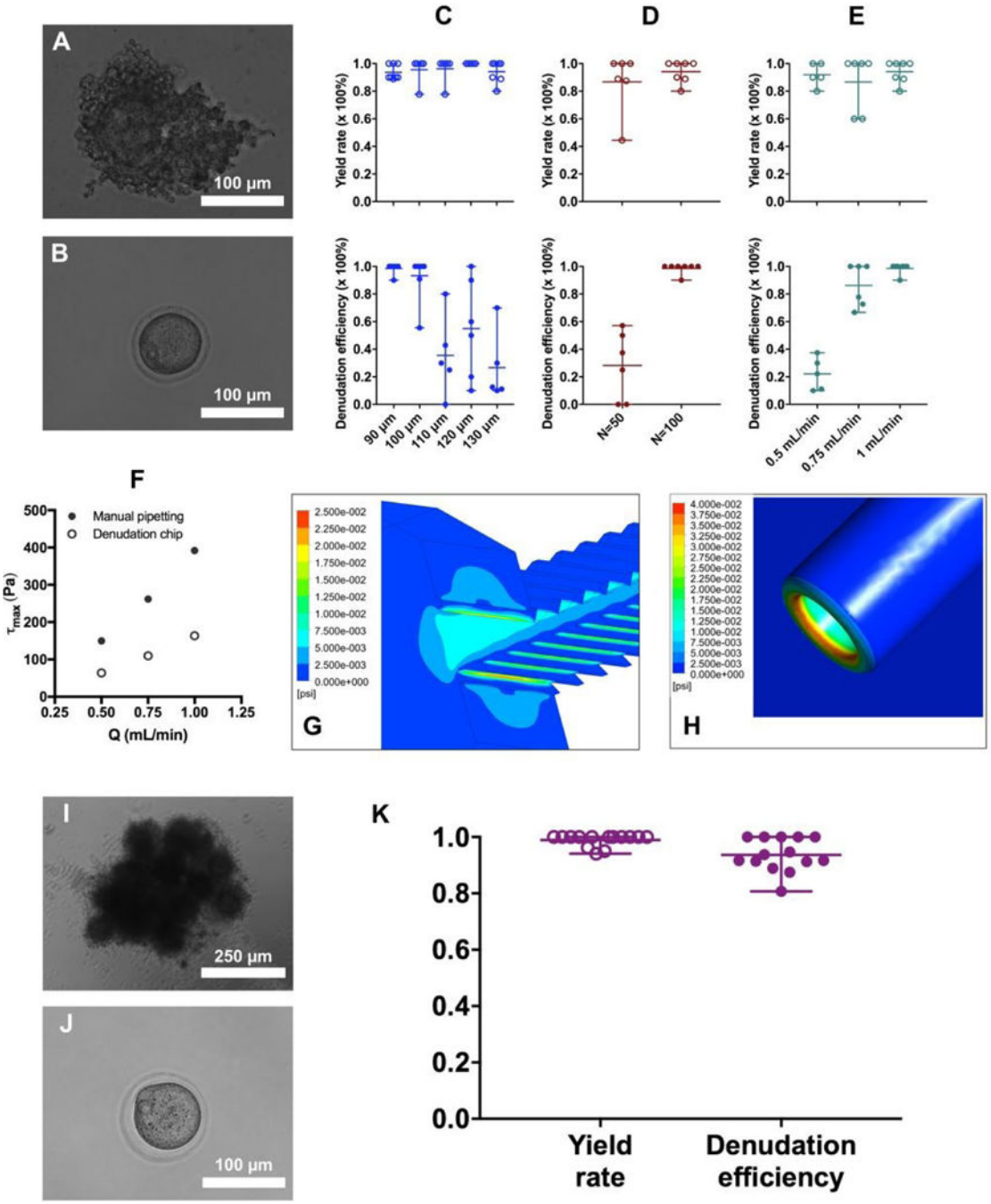

Figure 2.

Optimization of geometry and flow rate of the oocyte denudation device. (A) A GV stage mouse oocyte is buried within layers of cumulus cells. (B) A cumulus-free GV stage oocyte denuded by the device. (C) Effect of constriction width (W_3) on the yield rate and denudation efficiency (N and Q are 100 and 1 mL/min, respectively). (D) Effect of repeating number (N) on the yield rate and denudation efficiency (W_3 and Q are 90 μm and 1 mL/min, respectively). (E) Effect of flow rate (Q) on the yield rate and denudation efficiency (N and W_3 are 100 and 90 μm, respectively). (F) Maximum shear stress (τ_{max}) generated by on-chip

denudation or manual pipetting when applying different flow rates. (G) For the denudation device, the maximum shear acts at the edge of the first pair of teeth while the COC enters the constriction. (H) For manual pipetting, the maximum shear occurs at the inner ring of the capillary tip. (I) MII stage COCs present in a compact cluster before being treated with hyaluronidase. (J) A cumulus-free MII stage oocyte denuded by the device. (K) Yield rate and efficiency of the denudation device when processing MII stage COCs.

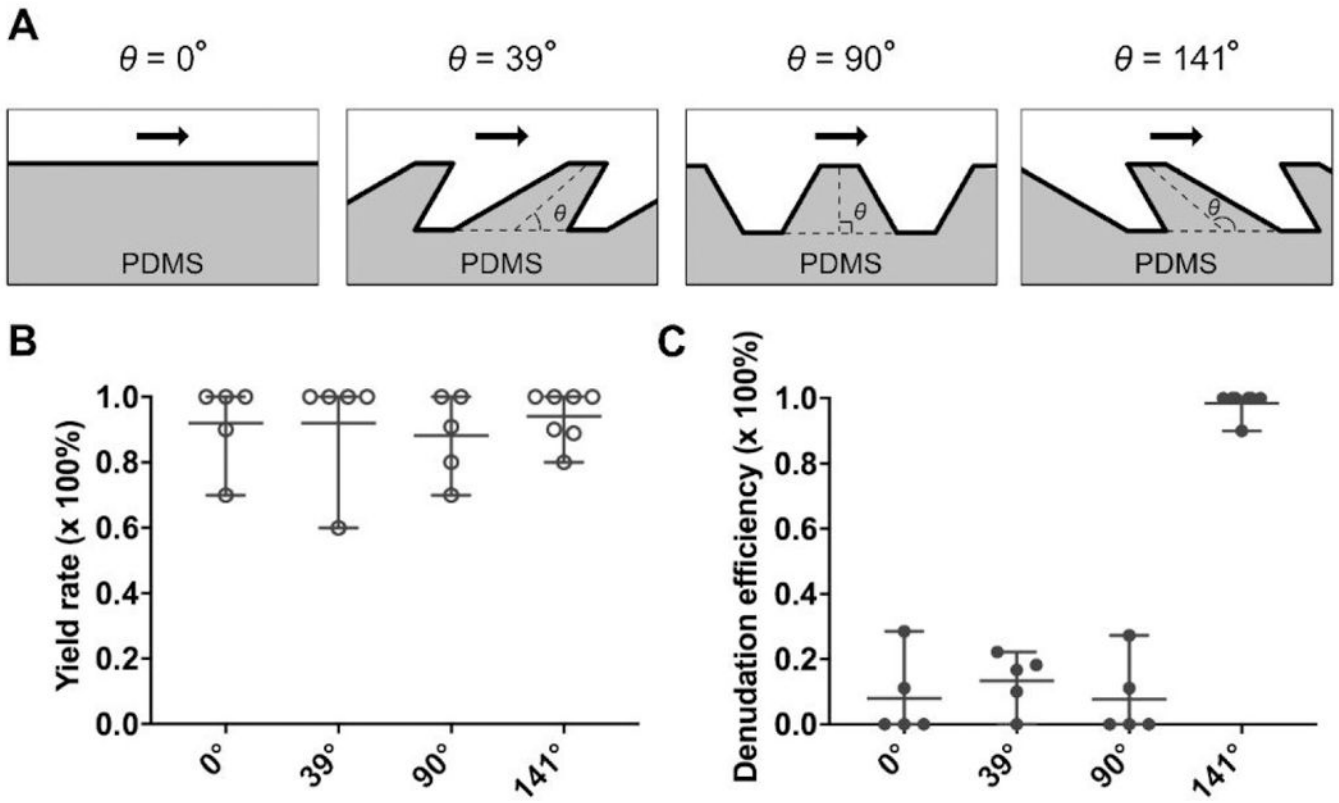

Figure 3.

Effect of teeth tilting angle (θ) on the denudation efficiency. (A) Illustration of four different conditions (θ=0°, 39°, 90° and 141°) of teeth tilting along the constriction channel. (B-C) Yield rate and denudation efficiency as a function of θ.

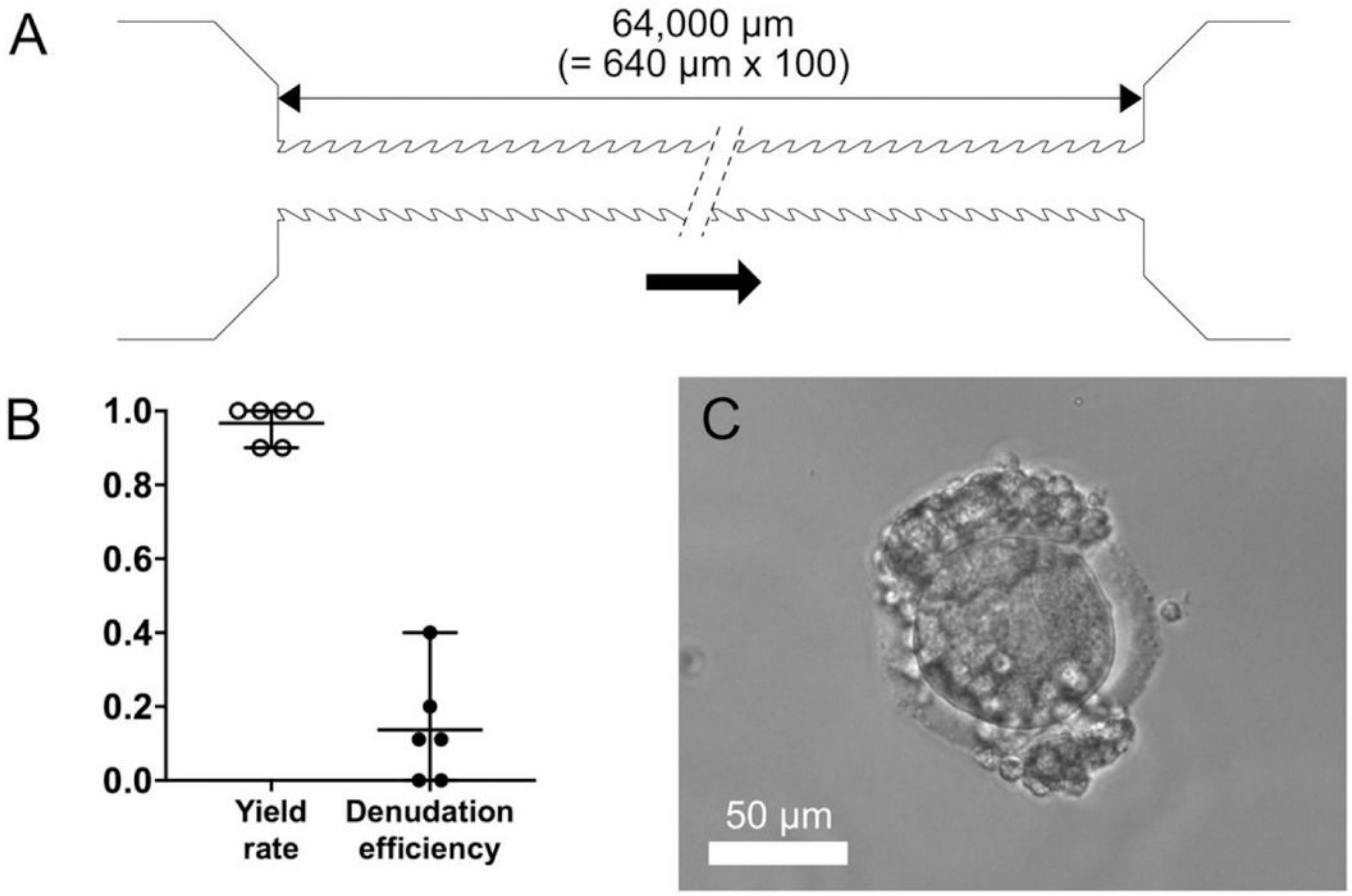

Figure 4.

Absence of repeating expansion channels has negative effect on denudation efficiency. (A) Illustration of a denudation device in which the last 100 constrictions (W_3=90 μm) are connected end to end without expansion breaks. (B) Yield rate and denudation efficiency achieved on the device shown in (A). (C) A representative image of a COC processed by the device that lacks the expansion channels in the third section.

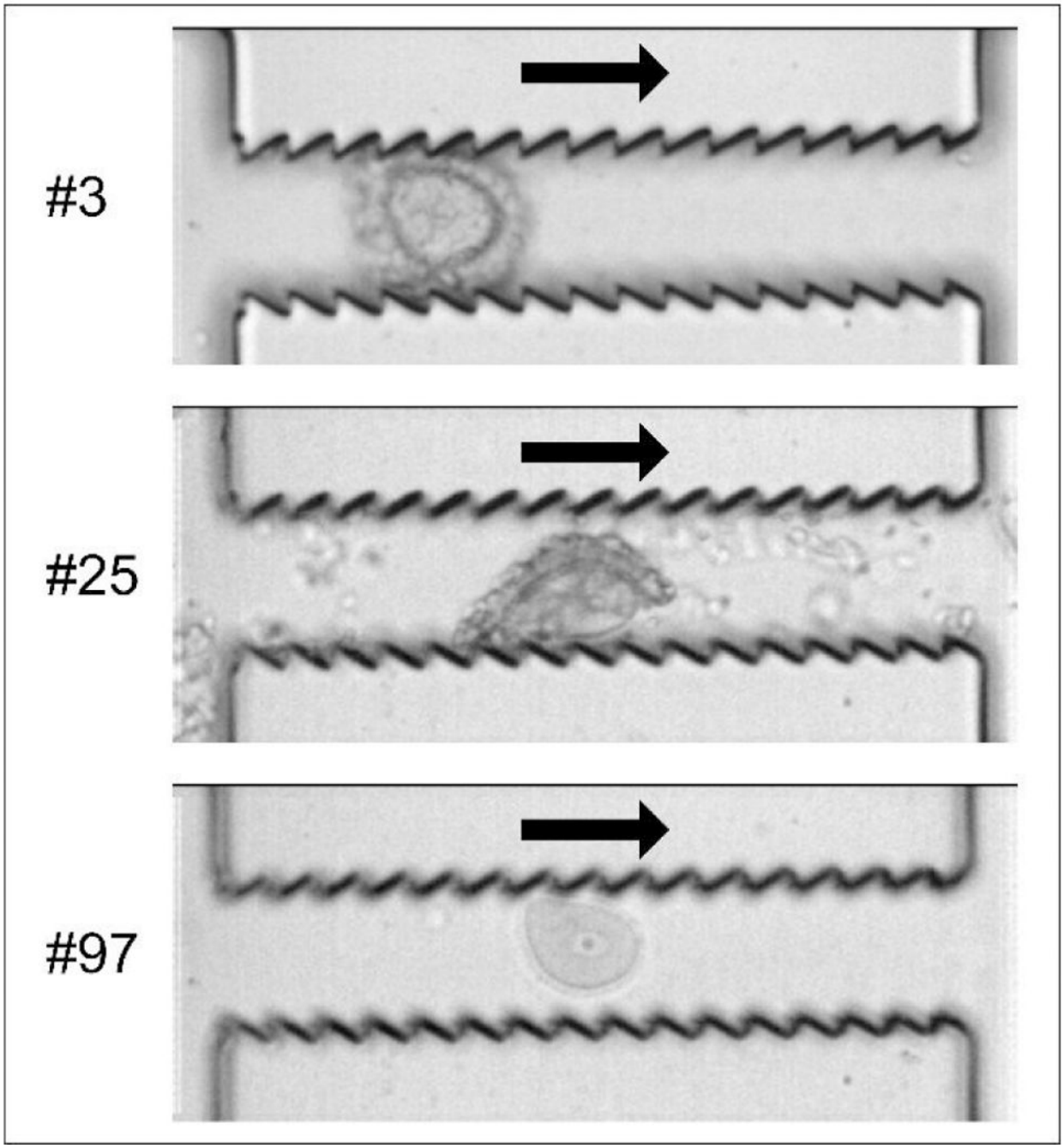

Figure 5.
Moments of oocyte denudation traveling through the jagged-surface constriction microchannels. An oocyte with cumulus-corona cells attached is traveling through the 3rd jagged- surface constriction channel (top); A second COC which has been partially denuded is traveling through the 25th constriction channel (middle); Another oocyte that has been fully denuded is traveling through the 97th channel (bottom).

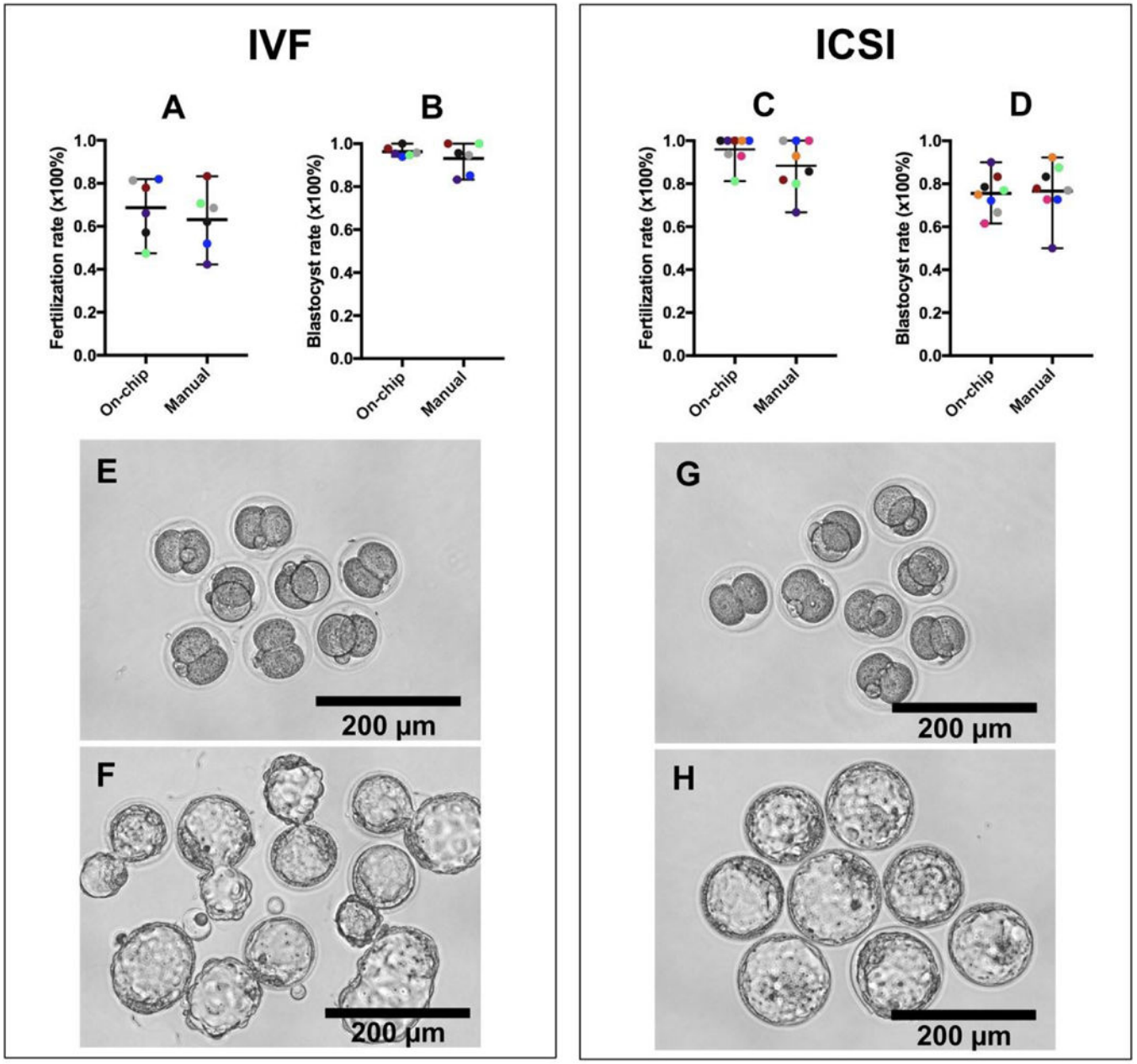

Figure 6.

Fertilization and development potentials are not comprised after the oocytes are denuded on the device. (A and B) Fertilization rate of oocytes inseminated via IVF and blastocyst rate of two-cell embryos. (C and D) Fertilization rate of oocytes injected by ICSI and blastocyst rate of two-cell embryos. The results for each repeat of either IVF or ICSI experiment have been represented by the same color. (E and F) Representative images of two-cell embryos (E) and blastocysts (F) including many hatching blastocysts produced by IVF. (G and H) Representative images of two-cell embryos (G) and blastocysts (H) produced by ICSI.